Communication

Axial-Ratio Bandwidth Enhancement of Circular-Polarized Bezel Antennas Using a Parasitic Capacitive Strip for Mobile Satellite Communications

Peihang Li, Yongjian Zhang, Xu Qin, Peiyu Liang, Kunpeng Wei, and Yue Li

***Abstract*— In this communication, a compact circularly polarized (CP) antenna with enhanced axial-ratio (AR) bandwidth is proposed for mobile satellite communications. This antenna utilizes a tri-dipole configuration deployed on the upper bezel of a mobile terminal with a small clearance. Due to the small distance to the mainboard, the radiation pattern of the dipole is deformed caused by the inbalanced currents on the two arms. To solve this problem, a capacitive balun is integrated with the dipole to co-direct the currents on the dipole and correct the radiation pattern. This balun structure also enhances the AR bandwidth while preserving the integrity of the main board. The fabricated prototype shows a 3 dB AR bandwidth of 195 MHz and a −6 dB impedance bandwidth of 360 MHz at 3.8 GHz within the clearance of 0.5 mm. Due to the merits of compact size, wide bandwidth, and balancing capability, the proposed antenna architecture is suitable for mobile terminal applications of satellite communications, demonstrating significant potential in space-constrained systems.**

***Index Terms*— Balun, circular polarization, mobile antennas, satellite communications, wideband antenna.**

I. Introduction

With the development of satellite-related technologies, satellite communications have become an essential component of global wireless communication networks. Examples include global positioning system (GPS) [1], [2], BeiDou [3], and Starlink [4]. Satellite communications can overcome the deployment difficulties of traditional base station wireless communications technology, extending services to remote areas such as oceans and deserts, and providing precise positioning services. Circularly polarized (CP) antennas are an attractive solution for satellite communication due to the atmospheric plasma layer [5], [6], which can deflect the polarization direction of linearly polarized antennas. In particular, satellite communications for mobile terminals have become a highly sought-after function. This demand is not limited to narrowband satellite positioning services but extends to broadband data transmission and Internet interaction. Therefore, designing a broadband, high-performance CP antenna suitable for mobile terminal satellite communications has become a significant research direction.

However, practical application scenarios for mobile terminals impose numerous constraints and challenges on the design of CP antennas. The antenna can only be designed within the bezel of the mobile terminal [7], [8], [9], and the main lobe of the antenna needs to be directed toward the sky to align with the satellite. Additionally, the compact space of mobile terminals limits the antenna size and requires the antenna to minimize its occupation of the mainboard [10], [11], [12], [13]. However, CP antennas are typically symmetric structures [14], [15], [16]. When using asymmetric feeding structures such as microstrip lines and coaxial lines [17], [18] in mobile terminals, a suitable balun such as choke loops [19], delay lines [20], [21], coupling structures [22], [23], [24], balun chips [25], and differential feeds [26] is required to balance the antenna current. This necessitates that the balun of the designed CP antenna occupies significant space to ensure current balance and beam symmetry, which contradicts the compact space available in mobile terminals. Consequently, most antenna designs for mobile terminal satellite communications involve compromises on various metrics, such as sacrificing bandwidth or encroaching on the space of the mainboard. For instance, in [27], high-quality circular polarization radiation was achieved using a dipole in a foldable phone. However, because the dipole is close to the mainboard, an additional balun structure of significant length was required to balance the currents on the two arms of the dipole. This design occupies a large clearance space, encroaching on the mainboard area of the mobile terminal. In [28], a low-clearance, wideband circular polarization radiation was achieved using a dipole array. However, due to the proximity of the structure to the mainboard, notches as a balun had to be introduced into the mainboard to balance the antenna current, thereby achieving better circular polarization radiation toward the satellite. Other works have implemented differential feeding using balun chips to achieve high-quality circular polarization radiation, but the bandwidth of the antenna remains limited [25]. In summary, designing a broadband and small-clearance CP antenna for satellite communication in the mobile terminals, while ensuring the integrity of the device mainboard, is still challenging due to the current balancing requirement for nondeformed radiation patterns.

In this communication, a compact balun structure utilizing parasitic capacitive strips is proposed, achieving the design of a small-clearance, wideband CP antenna that can be integrated into the upper bezel of a mobile terminal for satellite communications. The proposed antenna achieves wideband CP radiation through a tri-dipole configuration with a balun structure of parasitic capacitive strips, which co-directs the currents in the upper and lower arms of the dipole close to the ground, maintaining a small clearance of only 0.5 mm. The proposed balun structure not only balances the current but also broadens the antenna's bandwidth, achieving a 195 MHz axial ratio (AR) bandwidth within a compact size of $0.91\ \lambda_0 \times 0.07\ \lambda_0 \times 0.004\ \lambda_0$ at the center frequency. The antenna maintains a clearance of only 0.5 mm, preserving the integrity of the device mainboard. This design features wide bandwidth and small clearance, making it suitable for direct communication between satellites and mobile terminals.

Received 9 August 2024; revised 23 September 2024; accepted 28 October 2024. Date of publication 7 November 2024; date of current version 5 March 2025. This work was supported in part by the National Natural Science Foundation of China under Grant U22B2016, in part by the National Key Research and Development Program of China under Grant 2021YFA0716601, in part by China Postdoctoral Science Foundation under Grant GZB20240334 and Grant 2024M751678, and in part by Xiaomi Communications Company, Ltd. *(Corresponding author: Yue Li.)*

Peihang Li, Yongjian Zhang, Xu Qin, and Yue Li are with the Department of Electronic Engineering, Beijing National Research Center for Information Science and Technology, Tsinghua University, Beijing 100084, China (e-mail: lyee@tsinghua.edu.cn).

Peiyu Liang and Kunpeng Wei are with Xiaomi Communications Company Ltd., Beijing 100085, China.

Digital Object Identifier 10.1109/TAP.2024.3489887

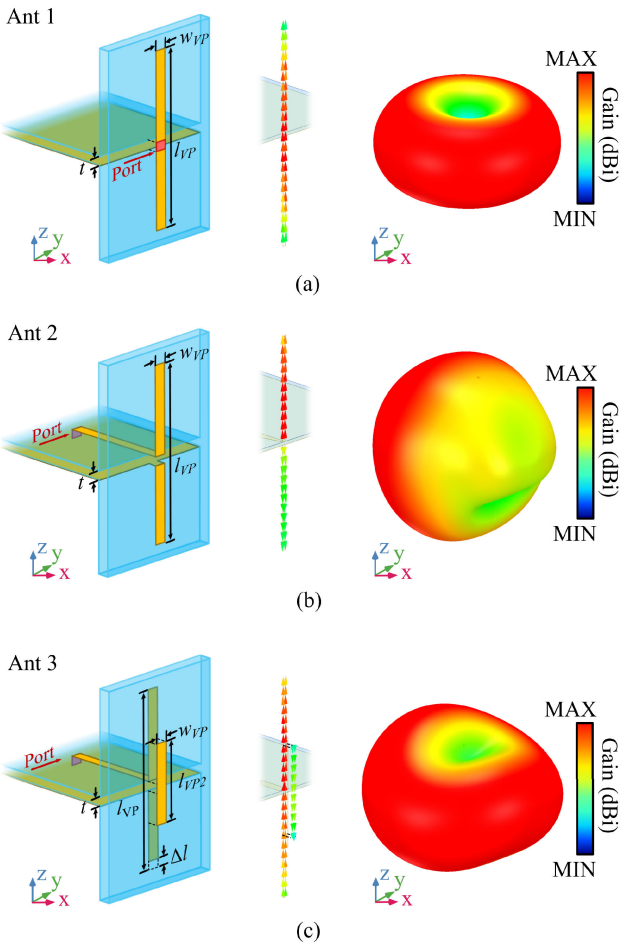

Fig. 1. Evolution of the proposed balun structure with corresponding radiation results. (a) Typical dipole antenna. (b) Dipole directly connected to a microstrip line. (c) Dipole antenna incorporating parasitic strip and introducing length differences. $t = 0.5$ mm, $w_{VP} = 0.5$ mm, $l_{VP} = 33$ mm, $l_{VP2} = 17$ mm, $\Delta l = 1$ mm.

II. Analysis of the Balun Structure

The proposed antenna comprises a balun structure and a tri-dipole configuration. This section presents an overview of the operational principles of the balun structure. The proposed balun structure aims to address the issue of current imbalance caused by the antenna being too close to the ground under extremely small clearance conditions [21]. As shown in Fig. 1(c), a parasitic capacitive strip is positioned across the upper and lower arms of the dipole, achieving current balance through coupled currents in the dipole arms.

To clearly demonstrate the working principle of the proposed balun, its structural evolution is presented in Fig. 1. Fig. 1(a) depicts a typical standard dipole, referred to as Ant 1, positioned near the ground with a clearance of 0.5 mm and a center frequency of 3.8 GHz. When excited by a symmetric lumped port, both the upper and lower arms of the dipole are uniformly excited, resulting in a uniform current distribution. Furthermore, considering a practical feeding scenario, when the dipole is excited through a microstrip line passing through the ground, the microstrip line connects to the upper arm of the dipole while the ground connects to the lower arm, named Ant 2, as shown in Fig. 1(b). Due to the asymmetric feeding structure of the microstrip line, most of the energy is supplied to the antenna through the upper arm, while the current in the lower arm of the dipole is shielded by the ground. This results in an inbalanced current

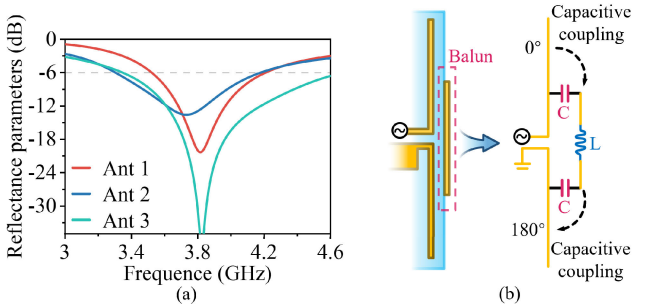

Fig. 2. (a) Impedance curves of Ant 1 to Ant 3. (b) Equivalent circuit diagram of the proposed balun structure.

distribution between the upper and lower arms of the dipole, causing the radiation pattern of the antenna to deteriorate from a dipole mode to a monopole mode. To balance the current distribution of Ant 2, traditional methods involve adding extension lines or cutting notches in the ground, which increase the size of the antenna or compromise the integrity of the mainboard. Ant 3 is proposed to achieve a compact current balance by placing a parasitic capacitive strip across the upper and lower arms of the dipole, as shown in Fig. 1(c). The length difference between the upper and lower arms of the dipole is introduced to readjust the impedance match. Compared to Ant 2, Ant 3 demonstrates a significant improvement in the current balance of the dipole. This improvement is also reflected in the radiation pattern of Ant 3, which resembles the nondeformed dipole radiation pattern.

Fig. 2(a) shows the impedance curves of Ant 1 through Ant 3. Compared to Ant 1, Ant 2 exhibits a frequency shift and degraded impedance bandwidth due to the current imbalance. The impedance bandwidth of Ant 3 is improved compared to Ant1, indicating that the proposed balun structure not only balances the dipole current but also enhances the radiation performance of the designed antenna. Fig. 2(b) shows the equivalent circuit diagram of the proposed balun structure. The additional parasitic capacitive strip can be modeled as a resonant structure bridging the upper and lower arms of the dipole, achieving a 180° phase shift of the upper and lower arms through the parasitic capacitive effect of the resonant structure. The distance between the parasitic strip and the dipole affects the equivalent capacitance, while the length of the parasitic strip influences the equivalent inductance. Since the distance t is typically determined by the thickness of the substrate, once the thickness is fixed, the length of the parasitic strip and the dipole can be adjusted to achieve the optimal current balance.

Fig. 3 shows the parameter study of the proposed balun structure. The current balancing capability of the proposed balun structure can be illustrated by the current phase difference between the upper and lower arms of the dipole; the closer the phase difference is to 180°, the more balanced the current distribution of the antenna. As shown in Fig. 3(b), as the length of l_{VP2} increases, the phase difference between the upper and lower arms of the dipole gradually approaches 180°, resulting in a more balanced current distribution. However, an excessively large l_{VP2} will negatively impact the designed antenna. When the l_{VP2} is too large, the length of the parasitic capacitive strip becomes comparable to the length of the dipole. In this case, the parasitic capacitive strip no longer acts as a balun but rather as a radiating structure, which can generate excessive reverse current, thereby reducing the radiation efficiency of the antenna and affecting its impedance matching, as shown in Fig. 3(b) and (c). Therefore, to avoid degradation in antenna efficiency and impedance matching while maintaining sufficient current balancing capability, the l_{VP2} of the proposed balun structure is set at 17 mm. Fig. 3(d) shows

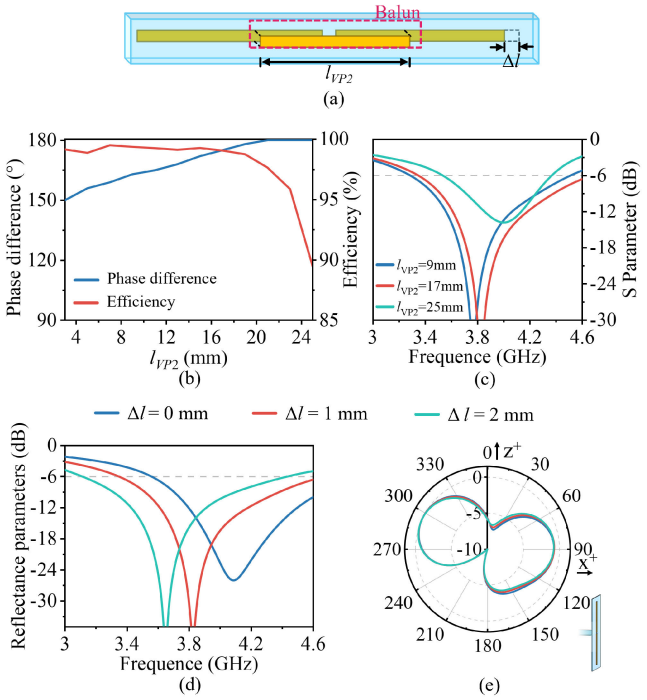

Fig. 3. (a) Schematic of the proposed balun structure. The phase difference between upper and lower arm currents, radiation efficiency (b) and impedance curves (c) of Ant 4 at different l_{VP2}. Impedance curves (d) and radiation patterns (e) of Ant 4 at different Δl.

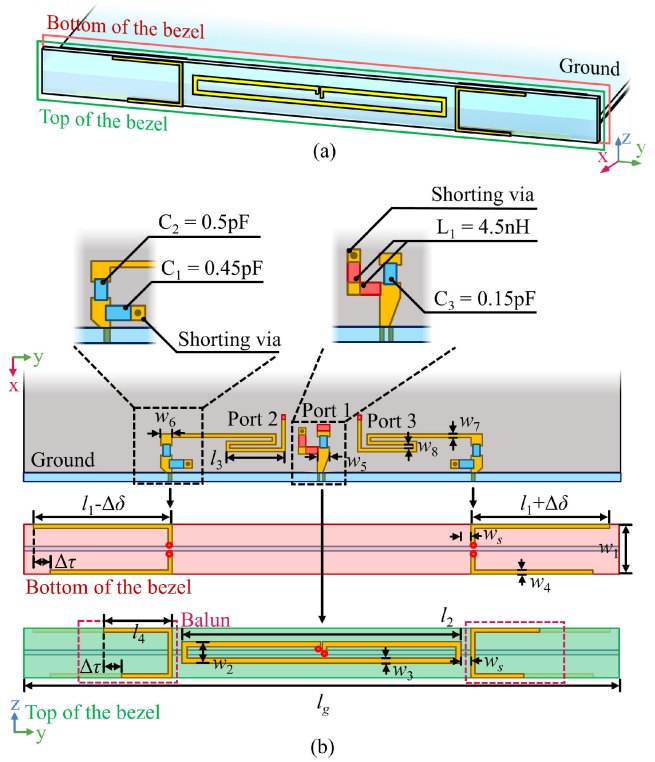

Fig. 4. Schematic of asymmetrical tri-dipoles CP antenna loaded with the proposed balun structure. (a) Isometric view. (b) Top view of the ground and bezel.

the effect of the length difference Δl on the impedance curve. As Δl increases, the center frequency of the antenna shifts to a lower frequency. The radiation patterns of the antenna under different Δl values are shown in Fig. 3(e), indicating that changing the Δl only affects the impedance of the antenna while not impacting its radiation pattern. Ultimately, Δl is determined to be 1 mm to compensate for the frequency shift caused by the parasitic capacitive strip.

Based on the research and analysis of the balun structure, the design approach of the proposed balun can be summarized as follows:

1) Determine the operating frequency and clearance of the antenna.
2) Set the length of the parasitic capacitive strip l_{VP2} to balance current distribution and maintain antenna efficiency.
3) Adjust the impedance matching of the antenna by fine-tuning parameter Δl between the upper and lower arms of the dipole.

It is worth noting that the proposed balun structure is applicable for current balancing in various dipoles, and multiple structures can achieve compact current balancing using this design approach [21], [26], [27], [29].

III. Configuration of the Antenna

Based on the proposed balun structure, this communication presents an optimized CP antenna design suitable for integration into the upper bezel of mobile terminals for satellite communications. As shown in Fig. 4, the antenna consists of a power division circuit on the ground and a radiating structure on the bezel. The substrate thickness is set to 0.508 mm, made of Rogers 5008 ($\varepsilon_r = 2.2$, $\tan\delta = 0.0009$). The relevant dimensions of the antenna are as follows: $l_1 = 17.4$ mm, $l_2 = 34.6$ mm, $l_3 = 9.2$ mm, $l_4 = 8.4$ mm, $l_g = 74$ mm, $w_1 = 6$ mm, $w_2 = 2.6$ mm, $w_3 = 0.6$ mm, $w_4 = 0.4$ mm, $w_5 = 1$ mm, $w_6 = 1$ mm, $w_7 = 0.15$ mm, $w_8 = 0.45$ mm, $w_s = 1.3$ mm, $\Delta\delta = 0.2$ mm, and $\Delta\tau = 2$ mm. The lumped elements used are model 0402 (1 × 0.5 mm). The back of the ground plane features a copper plate, which is considered to be the motherboard of the mobile terminal, simulating the electromagnetic environment in actual application scenarios.

The radiating structure of the proposed antenna consists of two bent vertical dipoles and one horizontal folded dipole, providing vertical polarized (VP) and horizontal polarized (HP) waves, respectively. These components are further combined into CP radiation through phase correction. The bent dipole can also balance the dipole current using the design method from Fig. 1. Two bent VP antennas are located at the bottom of the bezel, with the balun structures loaded on both sides of the top of the bezel to balance the current distribution of the VP antennas while maintaining the integrity of the mainboard. The VP antennas are excited by microstrip lines on both sides of the ground, with impedance matching achieved by adding capacitors C_1 and C_2 and a 90° phase difference is realized by an additional length of the delay line. As this work is primarily focused on prototype validation, the phase adjustment is performed using microstrip time delay lines. In practical applications, the phase shift can be achieved by loading elements [30], which can be equivalently combined with the port components in Fig. 4(b) for further integration. The HP folded dipole is located at the top of the bezel and achieves impedance matching through C_3 and L_1 on the mainboard. The proposed tri-dipole structure uses port 1–port 3 to feed the HP antenna and the two VP antennas, respectively. Considering that the three ports will eventually be combined into one port, the impedance of the three ports is set to 150 Ω, ensuring equal input power. In the subsequent practical antenna design, a 1-to-3 power splitter chip will be used to achieve equal power feeding for the three ports. Due to the inability to simulate the actual power splitter chip in the calculations, the simulation in this communication employs a three-port equal power feeding method to implement the design of the proposed antenna.

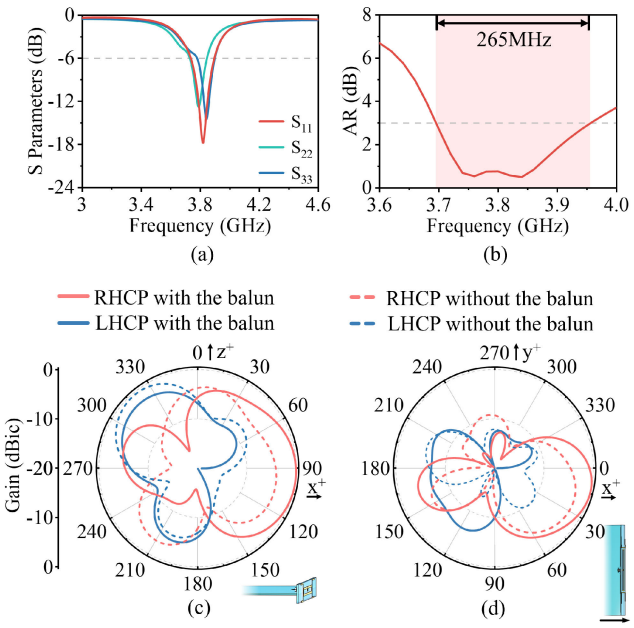

Fig. 5. Radiation performance of CP antenna loaded with proposed balun structure. (a) Impedance curves of the proposed antenna. (b) AR of the proposed antenna around the center frequency. (c) Radiation patterns at 3.8 GHz in $\phi = 0°$ plane (*xoz* plane). (d) Radiation patterns at 3.8 GHz in $\theta = 90°$ plane (*xoy* plane).

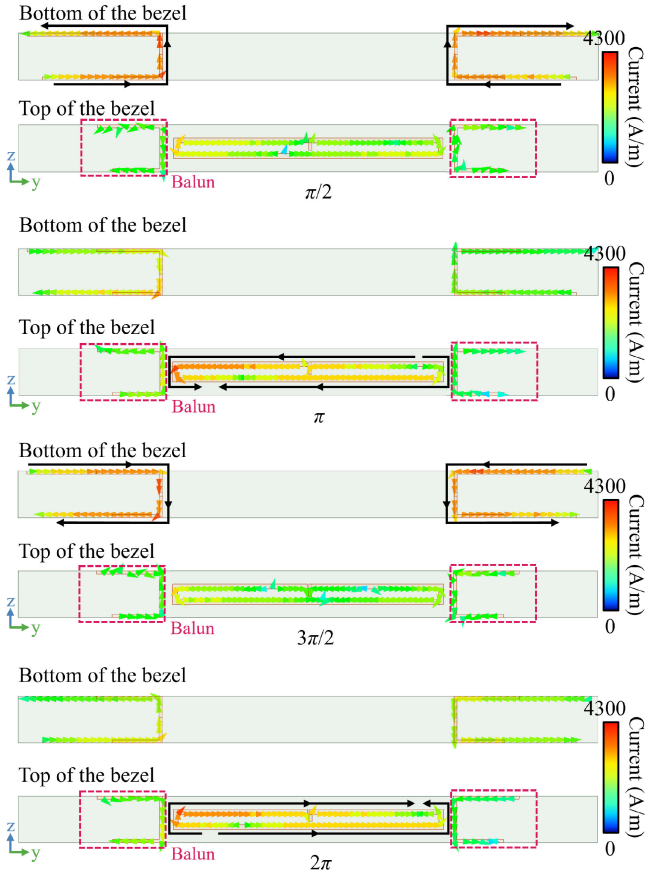

Fig. 6. Current distribution at center frequency of proposed antenna loaded with proposed balun structure in different phases.

Fig. 5(a) shows the simulated impedance curve results of the tri-dipole configuration with the parasitic capacitive strips. By introducing the asymmetry $\Delta\delta$ in the VP antennas, as shown in Fig. 4, the center frequency of the two VP antennas is intentionally offset. This approach optimizes the bandwidth of both the VP and HP antennas, thereby increasing the AR bandwidth of the proposed antenna. The balun structure at the top of the bezel is set to the optimal size and achieves excellent current balancing based on the theory introduced in Section II. The simulation results indicate that the proposed antenna achieves a 3 dB AR bandwidth of 265 MHz. Fig. 5(c) and (d) shows the simulated radiation patterns of the proposed antenna in the *xoz* plane and the *xoy* plane, respectively. The proposed balun structure balances the dipole current near the main board. Compared to the antenna without the balun structure, the antenna with the balun structure exhibits a more stable radiation pattern. Furthermore, the proposed antenna demonstrates satisfactory circular polarization radiation, with the main lobe of the main polarization right-hand circular polarization (RHCP) directed toward the bezel of the mobile terminal ($x+$ direction). Additionally, the proposed antenna features a wide beamwidth and broad AR bandwidth, making it suitable for wireless communication with low-orbit satellites in mobile terminals.

Fig. 6 shows the current distribution of the proposed antenna in different phases. The proposed tri-dipole configuration features bent VP dipoles on the sides that provide VP radiation, while the HP folded dipole in the middle provides HP radiation. The orthogonal polarizations from these components alternately reach their maximum values with a 90° phase difference, resulting in high-quality CP radiation. Throughout the entire period, the balun structure maintains a weak current distribution, indicating that the proposed balun functions effectively as a current balancing structure rather than a radiating structure.

IV. Fabrication and Measurements

To verify the feasibility of the proposed antenna, a prototype was fabricated, as shown in Fig. 7(a). The bezel and the mainboard are fixed together through a 10 mm rectangular groove reserved on the bezel. The proposed antenna prototype is fed through a 50 Ω coaxial cable and is excited by a power splitter chip, model SCG-3-392+, which provides equal power to the tri-dipole antenna on the bezel. The schematic of the power splitter chip is shown in Fig. 7(b). Due to the parasitic parameters inherent in the power splitter chip, an additional 1.8 nH inductor and 1.8 pF capacitor are arranged at the input port to compensate for the associated parasitic values. The measured gain of the proposed antenna is 2.54 dBic. Fig. 7(c) shows the measured impedance curve, indicating that the proposed antenna achieves a −6 dB impedance bandwidth of 360 MHz and a −10 dB impedance bandwidth of 142 MHz. The measured AR curve of the proposed antenna prototype, shown in Fig. 7(d), reveals an AR bandwidth of 195 MHz (5.13%). The antenna maintains good impedance matching within the −3 dB AR bandwidth frequency range. The efficiency of the antenna, shown in Fig. 7(e), demonstrates a maximum efficiency of 69.7% and remains consistently above 50% within the operating frequency band. The center frequency of the antenna prototype slightly shifts to a higher frequency, as shown in Fig. 7(e). However, overall, the simulation results and the test results of the proposed antenna show good agreement. Fig. 8 shows the simulated and measured far-field normalized radiation patterns of the proposed antenna. The discrepancies between the simulation and measurement results are attributed to the slight bending of the main board and manufacturing tolerances in the components. The main

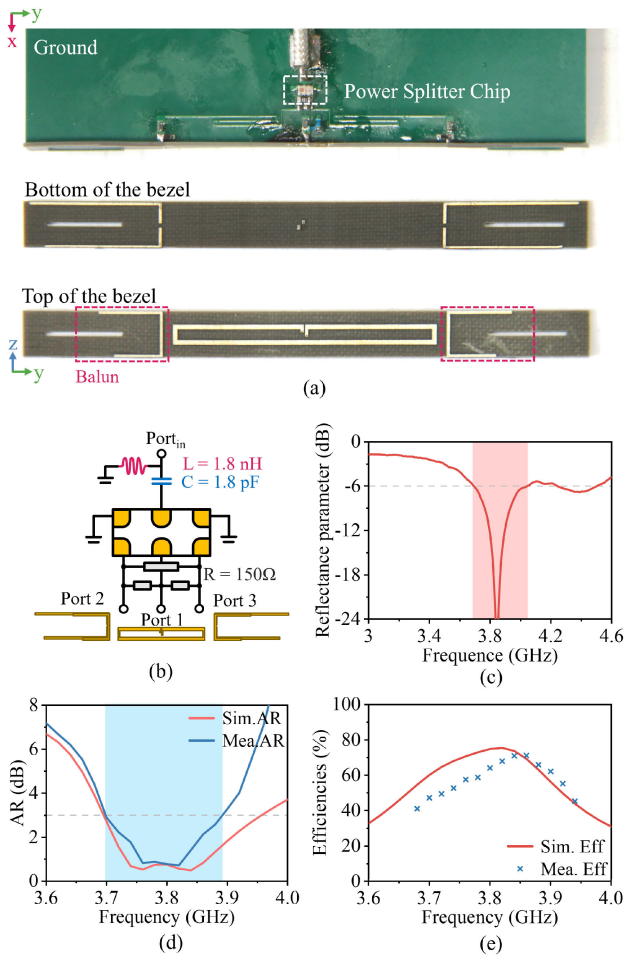

Fig. 7. Prototype and measurement results of CP antenna loaded with proposed balun structure. (a) Photographs of the proposed antenna prototype. (b) Circuit diagram of the power splitter chip. (c) Measured Impedance curves of the CP antenna with the proposed balun structure. (d) Simulated and measured the AR of the proposed antenna. (e) Simulated and measured the efficiency of the proposed antenna.

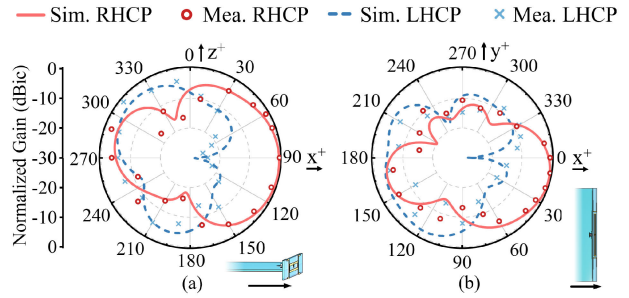

Fig. 8. Normalized radiation patterns at 3.8 GHz of the proposed antenna in (a) $\phi = 0^\circ$ plane (xoz plane) and (b) $\theta = 0^\circ$ plane (xoy plane).

polarization of the antenna is RHCP, with the main lobe directed toward the bezel of the mobile terminal ($x+$ direction), maintaining a wide beamwidth. This wide beamwidth facilitates beam alignment with satellites.

Table I summarizes the performance of the proposed antenna compared to other CP antennas. The impedance bandwidth is calculated with reference to -6 dB, and the AR bandwidth is calculated with reference to 3 dB, which are common criteria for mobile terminal antenna design. The clearance is defined as the distance from the outermost part of the radiation structure to the edge of the mainboard. Therefore, the data in Table I are based on this standard to ensure a fair comparison among different antennas. Clearly, the proposed antenna achieves satisfactory AR bandwidth performance while offering a small clearance and preserving the integrity of the mainboard. In [31], the designed antenna achieved good circular polarization radiation, but the additional clearance and square shape design hindered its application in mobile terminals. The antenna proposed in [32] also has excessive clearance and requires slotting of the mainboard. CP antenna designs for narrow bezels are realized in [8] and [25], maintaining minimal clearance and an intact mainboard. However, the AR bandwidth of these antennas is limited. In [28], a CP antenna design with a wide AR bandwidth was achieved using a tri-dipole configuration, but the extremely small clearance required additional notches in the mainboard to balance the dipole currents. In contrast, the antenna proposed in this work exhibits excellent CP radiation capability, wider AR bandwidth, and small clearance. By using parasitic capacitive strips as a novel balun structure, the proposed antenna achieves balanced current distribution with minimal clearance while maintaining the integrity of the mainboard, and it also extends the AR bandwidth.

TABLE I
COMPARISON OF CP ANTENNAS

Ref.	Size (λ_0^2)	Clearance (mm)	Gain (dBic)	Mainboard Integrity	Imp. BW	AR BW
[31]	0.14×0.14	15	4.75	Yes	4.7%	0.77%
[32]	0.49×0.25	10	3.4	No	6.1%	1.20%
[25]	0.53×0.06	2	1.90	Yes	2.4%	1.40%
[8]	0.46×0.06	1	4.80	Yes	10.0%	0.76%
[28]	0.88×0.07	0.5	2.42	No	17.8%	3.68%
T.W.	**0.91×0.07**	**0.5**	**2.54**	**Yes**	**9.47%**	**5.13%**

V. CONCLUSION

This communication proposes a small-clearance, wide AR bandwidth CP antenna with parasitic capacitive strips for satellite communication in mobile terminals. The proposed antenna consists of a tri-dipole configuration and parasitic capacitive strips. The tri-dipole configuration provides orthogonal polarizations and achieves a 90° phase difference through a delay line. The parasitic capacitive strips are attached to the bent VP dipoles on both sides. Serving as a novel balun structure, the parasitic capacitive strips co-direct currents in the dipole arms near the ground while extending the bandwidth. The proposed balun structure can achieve the current balance for near-ground dipoles with extremely small clearance. By incorporating this novel balun structure, the proposed antenna achieves CP radiation with minimal clearance while maintaining the integrity of the mainboard. Measurement results indicate that the proposed antenna achieves a 3 dB AR bandwidth of 195 MHz and a -6 dB impedance bandwidth of 360 MHz at 3.8 GHz within a clearance of 0.5 mm. Due to its compact size and wide AR bandwidth, the proposed antenna is an ideal candidate for satellite communication in mobile terminals.

REFERENCES

[1] D. Huang, Z. Du, and Y. Wang, "A quad-antenna system for 4G/5G/GPS metal frame mobile phones," *IEEE Antennas Wireless Propag. Lett.*, vol. 18, no. 8, pp. 1586–1590, Aug. 2019.

[2] X. Tian and Z. Du, "Dual-feed shared-radiator metal-frame full-screen mobile phone antenna for GPS and LTE bands with a dual-function capacitor," *IEEE Trans. Antennas Propag.*, vol. 71, no. 10, pp. 8314–8319, Oct. 2023.

[3] Y.-Y. Xu and Z.-H. Tu, "A compact dual-sense and dual-band circularly polarized antenna with wide axial-ratio beamwidth for BeiDou navigation satellite system," in *Proc. IEEE 11th Asia–Pacific Conf. Antennas Propag. (APCAP)*, Guangzhou, China, Nov. 2023, pp. 1–2.

[4] D. Laniewski, E. Lanfer, S. Beginn, J. Dunker, M. Dückers, and N. Aschenbruck, "Starlink on the road: A first look at mobile starlink performance in central Europe," in *Proc. 8th Netw. Traffic Meas. Anal. Conf. (TMA)*, Dresden, Germany, May 2024, pp. 1–8.

[5] B. K. Banerjea, "On the propagation of electromagnetic waves through the atmosphere," *Proc. Roy. Soc. London. Ser. A. Math. Phys. Sci.*, vol. 190, no. 1020, pp. 67–81, 1947.

[6] Z. Xu and Y. Wang, "Design of triple-band antenna for metal-bezel smartwatches with circular polarization in both GPS L5/L1 bands," *IEEE Trans. Antennas Propag.*, vol. 72, no. 3, pp. 2926–2931, Mar. 2024.

[7] W.-J. Lu, J.-W. Shi, K.-F. Tong, and H.-B. Zhu, "Planar endfire circularly polarized antenna using combined magnetic dipoles," *IEEE Antennas Wireless Propag. Lett.*, vol. 14, pp. 1263–1266, 2015.

[8] Z. Cao, L. Chang, Y. Li, K. Wei, and Z. Zhang, "Compact mobile terminal antenna with endfire circularly polarized beam for satellite communications," *IEEE Trans. Antennas Propag.*, vol. 71, no. 12, pp. 9980–9985, Dec. 2023.

[9] M. You, W.-J. Lu, B. Xue, L. Zhu, and H.-B. Zhu, "A novel planar endfire circularly polarized antenna with wide axial-ratio beamwidth and wide impedance bandwidth," *IEEE Trans. Antennas Propag.*, vol. 64, no. 10, pp. 4554–4559, Oct. 2016.

[10] W.-H. Zhang, W.-J. Lu, and K.-W. Tam, "A planar end-fire circularly polarized complementary antenna with beam in parallel with its plane," *IEEE Trans. Antennas Propag.*, vol. 64, no. 3, pp. 1146–1152, Mar. 2016.

[11] W. Zhao and Y. Wang, "A shared-branch eleven-band mobile antenna with a 0.5-mm clearance for metal-bezel mobile phones covering all the 4G LTE and 5G NR bands," *IEEE Trans. Antennas Propag.*, vol. 72, no. 4, pp. 3748–3753, Apr. 2024.

[12] B. Kim, J. Jung, S. Yun, H. Kim, and J. Oh, "Heterogeneous metasurface empowering proximate high-permittivity ceramic cover for a 5G dual-band millimeter-wave smartphone," *IEEE Trans. Antennas Propag.*, vol. 72, no. 5, pp. 4086–4094, May 2024.

[13] W. Yan et al., "Multimode balanced Mu-Near-Zero loop antenna for Wi-Fi 6/6E applications in full metal housing tablet computers," *IEEE Trans. Antennas Propag.*, vol. 72, no. 7, pp. 5469–5478, Jul. 2024.

[14] Y. Zhang, Y. Li, M. Hu, P. Wu, and H. Wang, "Dual-band circular-polarized microstrip antenna for ultrawideband positioning in smartphones with flexible liquid crystal polymer process," *IEEE Trans. Antennas Propag.*, vol. 71, no. 4, pp. 3155–3163, Apr. 2023.

[15] W. J. Yang, Y. M. Pan, and S. Y. Zheng, "Design of self-decoupled circularly polarized MIMO dielectric resonator antenna arrays based on polarization orthogonality," *IEEE Trans. Antennas Propag.*, vol. 72, no. 2, pp. 1192–1200, Feb. 2024.

[16] W. Zeng et al., "Broadband dual-CP multistage sequential rotation arrays with independent control of polarizations based on dual-CP magnetoelectric dipole elements," *IEEE Trans. Antennas Propag.*, vol. 72, no. 4, pp. 3017–3032, Apr. 2024.

[17] L. Sun, Y. Li, and Z. Zhang, "Wideband dual-polarized endfire antenna based on compact open-ended cavity for 5G mm-wave mobile phones," *IEEE Trans. Antennas Propag.*, vol. 70, no. 3, pp. 1632–1642, Mar. 2022.

[18] S. M. H. Mousavi, M. Moosazadeh, L. Guo, and A. M. Abbosh, "Compact dual-polarized cavity-backed antenna with wideband performance for deep torso imaging," *IEEE Trans. Antennas Propag.*, vol. 72, no. 3, pp. 2217–2227, Mar. 2024.

[19] T. Fukushima, N. Michishita, H. Morishita, and N. Fujimoto, "Coaxially fed monopole antenna with choke structure using left-handed transmission line," *IEEE Trans. Antennas Propag.*, vol. 65, no. 12, pp. 6856–6863, Dec. 2017.

[20] S. J. Yang, Y. F. Cao, Y. M. Pan, Y. Wu, H. Hu, and X. Y. Zhang, "Balun-fed dual-polarized broadband filtering antenna without extra filtering structure," *IEEE Antennas Wireless Propag. Lett.*, vol. 19, no. 4, pp. 656–660, Apr. 2020.

[21] J. X. Sun, M. Z. Chen, and Y. J. Cheng, "Single-PCB fabricated, ultrawideband, and wide-scanning phased array antenna with vertically integrated resistive frequency-selective surface," *IEEE Trans. Antennas Propag.*, vol. 72, no. 3, pp. 2411–2422, Mar. 2024.

[22] Y. Zhang, Y. Li, W. Zhang, Z. Zhang, and Z. Feng, "Omnidirectional antenna diversity system for high-speed onboard communication," *Engineering*, vol. 11, pp. 72–79, Apr. 2022.

[23] H. Li, Z. Zhou, Y. Zhao, and Y. Li, "Low-loss beam synthesizing network based on Epsilon-near-zero (ENZ) medium for on-chip antenna array," *Chip*, vol. 2, no. 2, Jun. 2023, Art. no. 100049.

[24] Y. Zhang and Y. Li, "Wideband microstrip antenna in small volume without using fundamental mode," *Electromagn. Sci.*, vol. 1, no. 2, pp. 1–6, Jun. 2023.

[25] X. Zhang, K. Wei, Y. Li, and Z. Zhang, "A circularly polarized antenna based on narrowed crossed dipole for smartphone satellite communication," *IEEE Antennas Wireless Propag. Lett.*, vol. 23, pp. 2511–2515, 2024.

[26] Y.-Y. Zhu, J. Wang, J.-X. Chen, and W. Wu, "A compact wideband dual-polarized antenna using monolithic dielectric for 5G base station application," *IEEE Antennas Wireless Propag. Lett.*, vol. 21, pp. 1717–1721, 2022.

[27] X. Zhang, K. Wei, Y. Li, and Z. Zhang, "A polarization reconfigurable antenna for satellite communication in foldable smartphone," *IEEE Trans. Antennas Propag.*, vol. 71, no. 12, pp. 9938–9943, Dec. 2023.

[28] P. Li, Y. Zhang, X. Qin, K. Wei, P. Liang, and Y. Li, "Wideband widebeam circular-polarized antenna using asymmetrical tri-dipoles for direct satellite-to-handset communication," *IEEE Trans. Antennas Propagat.*, vol. 72, no. 8, pp. 6270–6277, Aug. 2024, doi: 10.1109/TAP.2024.3420086.

[29] A. Li, S.-W. Qu, and S. Yang, "Conformal array antenna for applications in wide-scanning phased array antenna systems," *IEEE Antennas Wireless Propag. Lett.*, vol. 21, pp. 1762–1766, 2022.

[30] Y. Zhang and Y. Li, "Wideband isotropic antenna with miniaturized ground for enhanced 3 dB coverage ratio," *IEEE Antennas Wireless Propag. Lett.*, vol. 21, no. 6, pp. 1253–1257, Jun. 2022.

[31] Z. Wang, S. Liu, and Y. Dong, "Electrically small, low-Q, wide beam-width, circularly polarized, hybrid magnetic dipole antenna for RFID application," *IEEE Trans. Antennas Propag.*, vol. 69, no. 10, pp. 6284–6293, Oct. 2021.

[32] L. Guo, "Compact wide-beam circularly polarized end-fire antenna combining ground radiation mode and vertically polarized mode," *IEEE Trans. Antennas Propag.*, vol. 70, no. 11, pp. 10218–10225, Nov. 2022.